Search for lepton-flavor violation in e^+p collisions at DESY HERA

S. Chekanov, M. Derrick, D. Krakauer, S. Magill, B. Musgrave, A. Pellegrino, J. Repond, and R. Yoshida
Argonne National Laboratory, Argonne, Illinois 60439-4815

M. C. K. Mattingly
Andrews University, Berrien Springs, Michigan 49104-0380

P. Antonioli, G. Bari, M. Basile, L. Bellagamba, D. Boscherini, A. Bruni, G. Bruni, G. Cara Romeo, L. Cifarelli, F. Cindolo, A. Contin, M. Corradi, S. De Pasquale, P. Giusti, G. Iacobucci, G. Levi, A. Margotti, T. Massam, R. Nania, F. Palmonari, A. Pesci, G. Sartorelli, and A. Zichichi
University and INFN Bologna, Bologna, Italy

G. Aghuzumtsyan, D. Bartsch, I. Brock, J. Crittenden,[a] S. Goers, H. Hartmann, E. Hilger, P. Irrgang, H.-P. Jakob, A. Kappes, U. F. Katz,[b] R. Kerger, O. Kind, E. Paul, J. Rautenberg, R. Renner, H. Schnurbusch, A. Stifutkin, J. Tandler, K. C. Voss, A. Weber, and H. Wessoleck
Physikalisches Institut der Universität Bonn, Bonn, Germany

D. S. Bailey, N. H. Brook, J. E. Cole, B. Foster, G. P. Heath, H. F. Heath, S. Robins, E. Rodrigues, J. Scott, R. J. Tapper, and M. Wing
H.H. Wills Physics Laboratory, University of Bristol, Bristol, United Kingdom

M. Capua, A. Mastroberardino, M. Schioppa, and G. Susinno
Calabria University, Physics Department and INFN, Cosenza, Italy

H. Y. Jeoung, J. Y. Kim, J. H. Lee, I. T. Lim, K. J. Ma, and M. Y. Pac[c]
Chonnam National University, Kwangju, Korea

A. Caldwell, M. Helbich, X. Liu, B. Mellado, S. Paganis, W. B. Schmidke, and F. Sciulli
Nevis Laboratories, Columbia University, Irvington on Hudson, New York 10027

J. Chwastowski, A. Eskreys, J. Figiel, K. Olkiewicz, M. B. Przybycień,[d] P. Stopa, and L. Zawiejski
Institute of Nuclear Physics, Cracow, Poland

B. Bednarek, I. Grabowska-Bold, K. Jeleń, D. Kisielewska, A. M. Kowal, M. Kowal, T. Kowalski, B. Mindur, M. Przybycień, E. Rulikowska-Zarębska, L. Suszycki, D. Szuba, and J. Szuba
Faculty of Physics and Nuclear Techniques, University of Mining and Metallurgy, Cracow, Poland

A. Kotański and W. Słomiński[e]
Department of Physics, Jagellonian University, Cracow, Poland

L. A. T. Bauerdick,[f] U. Behrens, K. Borras, V. Chiochia, D. Dannheim, K. Desler,[g] G. Drews, J. Fourletova, A. Fox-Murphy, U. Fricke, A. Geiser, F. Goebel, P. Göttlicher, R. Graciani, T. Haas, W. Hain, G. F. Hartner, S. Hillert, U. Kötz, H. Kowalski, H. Labes, D. Lelas, B. Löhr, R. Mankel, J. Martens,[h] M. Martínez,[f] M. Moritz, D. Notz, M. C. Petrucci, A. Polini, U. Schneekloth, F. Selonke, S. Stonjek, B. Surrow,[i] J. J. Whitmore,[j] R. Wichmann,[k] G. Wolf, C. Youngman, and W. Zeuner
Deutsches Elektronen-Synchrotron DESY, Hamburg, Germany

C. Coldewey,[l] A. Lopez-Duran Viani, A. Meyer, and S. Schlenstedt
DESY Zeuthen, Zeuthen, Germany

G. Barbagli, E. Gallo, C. Genta, and P. G. Pelfer
University and INFN, Florence, Italy

A. Bamberger, A. Benen, N. Coppola, P. Markun, H. Raach, and S. Wölfle
Fakultät für Physik der Universität Freiburg i.Br., Freiburg i.Br., Germany

M. Bell, P. J. Bussey, A. T. Doyle, C. Glasman, S. Hanlon, S. W. Lee, A. Lupi, G. J. McCance, D. H. Saxon, and I. O. Skillicorn

Department of Physics and Astronomy, University of Glasgow, Glasgow, United Kingdom

B. Bodmann, U. Holm, H. Salehi, K. Wick, A. Ziegler, and Ar. Ziegler
Hamburg University, I. Institute of Experimental Physics, Hamburg, Germany

T. Carli, I. Gialas,[m] K. Klimek, E. Lohrmann, and M. Milite
Hamburg University, II. Institute of Experimental Physics, Hamburg, Germany

C. Collins-Tooth, C. Foudas, R. Gonçalo, K. R. Long, F. Metlica, D. B. Miller, A. D. Tapper, and R. Walker
Imperial College London, High Energy Nuclear Physics Group, London, United Kingdom

P. Cloth and D. Filges
Forschungszentrum Jülich, Institut für Kernphysik, Jülich, Germany

M. Kuze, K. Nagano, K. Tokushuku,[n] S. Yamada, and Y. Yamazaki
Institute of Particle and Nuclear Studies, KEK, Tsukuba, Japan

A. N. Barakbaev, E. G. Boos, N. S. Pokrovskiy, and B. O. Zhautykov
Institute of Physics and Technology of Ministry of Education and Science of Kazakhstan, Almaty, Kazakhstan

S. H. Ahn, S. B. Lee, and S. K. Park
Korea University, Seoul, Korea

H. Lim and D. Son
Kyungpook National University, Taegu, Korea

F. Barreiro, G. García, O. González, L. Labarga, J. del Peso, I. Redondo, J. Terrón, and M. Vázquez
Departamento de Física Teórica, Universidad Autónoma Madrid, Madrid, Spain

M. Barbi, A. Bertolin, F. Corriveau, A. Ochs, S. Padhi, D. G. Stairs, and M. St-Laurent
Department of Physics, McGill University, Montréal, Québec, Canada H3A 2T8

T. Tsurugai
Meiji Gakuin University, Faculty of General Education, Yokohama, Japan

A. Antonov, V. Bashkirov,[o] P. Danilov, B. A. Dolgoshein, D. Gladkov, V. Sosnovtsev, and S. Suchkov
Moscow Engineering Physics Institute, Moscow, Russia

R. K. Dementiev, P. F. Ermolov, Yu. A. Golubkov, I. I. Katkov, L. A. Khein, N. A. Korotkova, I. A. Korzhavina, V. A. Kuzmin, B. B. Levchenko, O. Yu. Lukina, A. S. Proskuryakov, L. M. Shcheglova, A. N. Solomin, N. N. Vlasov, and S. A. Zotkin
Moscow State University, Institute of Nuclear Physics, Moscow, Russia

C. Bokel, J. Engelen, S. Grijpink, E. Koffeman, P. Kooijman, E. Maddox, S. Schagen, E. Tassi, H. Tiecke, N. Tuning, J. J. Velthuis, L. Wiggers, and E. de Wolf
NIKHEF and University of Amsterdam, Amsterdam, Netherlands

N. Brümmer, B. Bylsma, L. S. Durkin, J. Gilmore, C. M. Ginsburg, C. L. Kim, and T. Y. Ling
Physics Department, Ohio State University, Columbus, Ohio 43210

S. Boogert, A. M. Cooper-Sarkar, R. C. E. Devenish, J. Ferrando, T. Matsushita, M. Rigby, O. Ruske,[p] M. R. Sutton, and R. Walczak
Department of Physics, University of Oxford, Oxford, United Kingdom

R. Brugnera, R. Carlin, F. Dal Corso, S. Dusini, A. Garfagnini, S. Limentani, A. Longhin, A. Parenti, M. Posocco, L. Stanco, and M. Turcato
Dipartimento di Fisica dell' Università and INFN, Padova, Italy

L. Adamczyk, B. Y. Oh, and P. R. B. Saull
Department of Physics, Pennsylvania State University, University Park, Pennsylvania 16802

Y. Iga
Polytechnic University, Sagamihara, Japan

G. D'Agostini, G. Marini, and A. Nigro
Dipartimento di Fisica, Università "La Sapienza" and INFN, Rome, Italy

C. Cormack, J. C. Hart, and N. A. McCubbin
Rutherford Appleton Laboratory, Chilton, Didcot, Oxon, United Kingdom

C. Heusch
University of California, Santa Cruz, California 95064

I. H. Park
Seoul National University, Seoul, Korea

N. Pavel
Fachbereich Physik der Universität-Gesamthochschule Siegen, Germany

H. Abramowicz, S. Dagan, A. Gabareen, S. Kananov, A. Kreisel, and A. Levy
Raymond and Beverly Sackler Faculty of Exact Sciences, School of Physics, Tel-Aviv University, Tel-Aviv, Israel

T. Abe, T. Fusayasu, T. Kohno, K. Umemori, and T. Yamashita
Department of Physics, University of Tokyo, Tokyo, Japan

R. Hamatsu, T. Hirose, M. Inuzuka, S. Kitamura,[q] K. Matsuzawa, and T. Nishimura
Department of Physics, Tokyo Metropolitan University, Tokyo, Japan

M. Arneodo,[r] N. Cartiglia, R. Cirio, M. Costa, M. I. Ferrero, S. Maselli, V. Monaco, C. Peroni, M. Ruspa, R. Sacchi, A. Solano, and A. Staiano
Università di Torino, Dipartimento di Fisica Sperimentale and INFN, Torino, Italy

R. Galea, T. Koop, G. M. Levman, J. F. Martin, A. Mirea, and A. Sabetfakhri
Department of Physics, University of Toronto, Toronto, Ontario, Canada M5S 1A7

J. M. Butterworth, C. Gwenlan, R. Hall-Wilton, M. E. Hayes,[s] E. A. Heaphy, T. W. Jones, J. B. Lane, M. S. Lightwood, and B. J. West
Physics and Astronomy Department, University College London, London, United Kingdom

J. Ciborowski,[t] R. Ciesielski, G. Grzelak, R. J. Nowak, J. M. Pawlak, B. Sṃalska, J. Sztuk,[u] T. Tymieniecka, A. Ukleja, J. Ukleja, J. A. Zakrzewski, and A. F. Żarnecki
Warsaw University, Institute of Experimental Physics, Warsaw, Poland

M. Adamus and P. Plucinski
Institute for Nuclear Studies, Warsaw, Poland

Y. Eisenberg, L. K. Gladilin,[v] D. Hochman, and U. Karshon
Department of Particle Physics, Weizmann Institute, Rehovot, Israel

J. Breitweg,[w] D. Chapin, R. Cross, D. Kçira, S. Lammers, D. D. Reeder, A. A. Savin, and W. H. Smith
Department of Physics, University of Wisconsin, Madison, Wisconsin 53706

A. Deshpande, S. Dhawan, V. W. Hughes, and P. B. Straub
Department of Physics, Yale University, New Haven, Connecticut 06520-8121

S. Bhadra, C. D. Catterall, S. Fourletov, S. Menary, M. Soares, and J. Standage
Department of Physics, York University, Ontario, Canada M3J 1P3

(Zeus Collaboration)
(Received 8 January 2002; published 24 April 2002)

A search has been made for lepton-flavor-violating interactions of the type $e^+p \to lX$, where l denotes a μ or τ with high transverse momentum, at a center-of-mass energy $\sqrt{s}$ of 300 GeV with an integrated luminosity of 47.7 pb^{-1} using the ZEUS detector at HERA. No evidence was found for lepton-flavor violation and constraints were derived on leptoquarks (LQs) that could mediate such interactions. For LQ masses below $\sqrt{s}$, limits are set on $\lambda_{eq_1}\sqrt{\beta_{lq}}$, where λ_{eq_1} is the coupling of the LQ to an electron and a first-generation quark q_1 and β_{lq} is the branching ratio of the LQ to l and a quark. For LQ masses exceeding $\sqrt{s}$, limits are set on the four-fermion contact-interaction term $\lambda_{eq_\alpha}\lambda_{lq_\beta}/M_{\mathrm{LQ}}^2$ for leptoquarks that couple to an electron and a quark q_α and also to l and a quark q_β. Some of the limits are also applicable to lepton-flavor-violating processes mediated by squarks in *R*-parity-violating supersymmetric models. In some cases involving heavy quarks and especially for $l=\tau$, the ZEUS limits are the most stringent published to date.

DOI: 10.1103/PhysRevD.65.092004 PACS number(s): 13.10.+q, 14.80.Ly

I. INTRODUCTION

In the standard model (SM), lepton flavor is conserved. While the reported observation of neutrino oscillations [1,2] implies that lepton-flavor violation (LFV) does occur, minimal extensions to the SM [3] that allow for finite neutrino masses and thereby account for neutrino oscillations do not predict detectable rates of LFV at current collider experiments. However, many extensions of the SM, such as grand unified theories [4], models based on supersymmetry [5], compositeness [6], or technicolor [7] involve LFV interactions at fundamental levels.

In high-energy positron-proton collisions at the DESY *ep* collider HERA, reactions of the type $eq_i \to lq_f$, where q_i and q_f denote initial- and final-state quarks and l denotes a μ or a τ with high transverse momentum, can be detected with high efficiency and small background. Indirect searches for such reactions have yielded very strong constraints [8] for cases where q_i and q_f are light quarks. However, in some cases involving heavy quarks, especially when $l=\tau$, the sensitivity of HERA extends beyond existing low-energy limits.

This paper reports on a search for LFV processes in e^+p collisions using data collected by the ZEUS experiment from 1994 to 1997 with an integrated luminosity $\mathcal{L}$ of 47.7 pb^{-1}. The data were taken at a center-of-mass energy of 300 GeV, with a positron beam of 27.5 GeV and a proton beam of 820 GeV. Previous searches for LFV at HERA have been reported by ZEUS [9] ($\mathcal{L}\sim 4$ pb^{-1}) and H1 [10] ($\mathcal{L}\sim 37$ pb^{-1}).

II. PHENOMENOLOGY

There are several mechanisms whereby lepton flavor can be violated in *ep* collisions. This paper considers two main possibilities: leptoquarks and *R*-parity-violating squarks.

A. Leptoquarks

Leptoquarks (LQs) are bosons that carry both lepton (L) and baryon (B) numbers and have lepton-quark Yukawa couplings. Such bosons arise naturally in unified theories that arrange quarks and leptons in common multiplets. A LQ that couples to leptons of two different generations would induce LFV. The Buchmüller-Rückl-Wyler (BRW) model [11], which assumes the most general Lagrangian with $\mathrm{SU(3)_C} \times \mathrm{SU(2)_L} \times \mathrm{U(1)_Y}$ invariant couplings of a LQ to a lepton and a quark, is used to classify LQ species and to calculate cross sections for LQ-mediated processes. The following additional assumptions were made to simplify the models under consideration:

(1) One LQ species dominates the cross section of the process.

(2) Members of each SU(2) multiplet are degenerate in mass.

(3) LQs couple to either left-handed or right-handed leptons, but not both.

[a]Now at Cornell University, Ithaca, N.Y.
[b]On leave of absence at University of Erlangen-Nürnberg, Germany.
[c]Now at Dongshin University, Naju, Korea.
[d]Now at Northwestern University, Evanston, IL.
[e]Also at Department of Computer Science, Jagellonian University, Cracow, Poland.
[f]Now at Fermilab, Batavia, IL.
[g]Now at DESY group MPY.
[h]Now at Philips Semiconductors, Hamburg, Germany.
[i]Now at Brookhaven National Laboratory, Upton, N.Y.
[j]On leave from Penn State University, University Park, PA.
[k]Now at Mobilcom AG, Rendsburg-Büdelsdorf, Germany.
[l]Now at GFN Training GmbH, Hamburg, Germany.
[m]Also at University of the Aegean, Mytilene, Greece.
[n]Also at University of Tokyo, Tokyo, Japan.
[o]Now at Loma Linda University, Loma Linda, CA.
[p]Now at IBM Global Services, Frankfurt au Main, Germany.
[q]Present address: Tokyo Metropolitan University of Health Sciences, Tokyo 116-8551, Japan.
[r]Also at Università del Piemonte Orientale, Novara, Italy.
[s]Now at CERN, Geneva, Switzerland.
[t]Also at Łódź University, Lódź, Poland.
[u]Also at Łódź University, Lódź, Poland.
[v]On leave from MSU.
[w]Now at EssNet Deutschland GmbH, Hamburg, Germany.

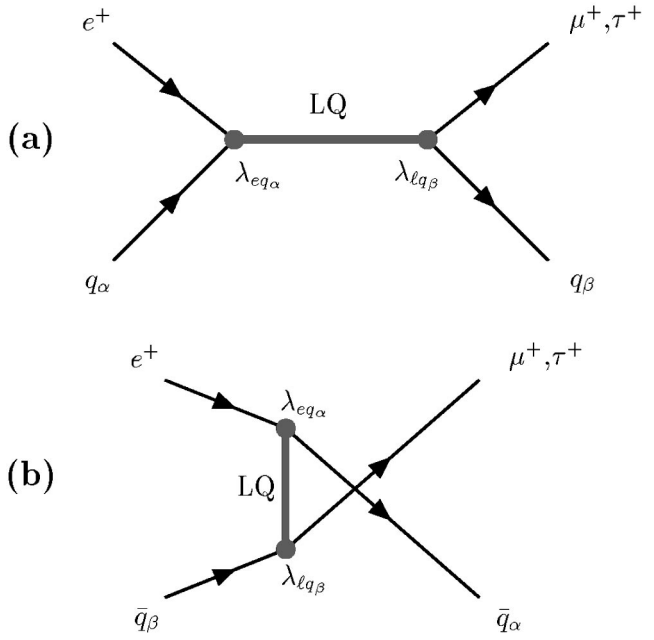

FIG. 1. (a) *s*-channel and (b) *u*-channel diagrams contributing to LFV processes induced by $F=0$ LQs. In e^+p scattering, $|F|=2$ LQs couple to antiquarks in the *s* channel and to quarks in the *u* channel.

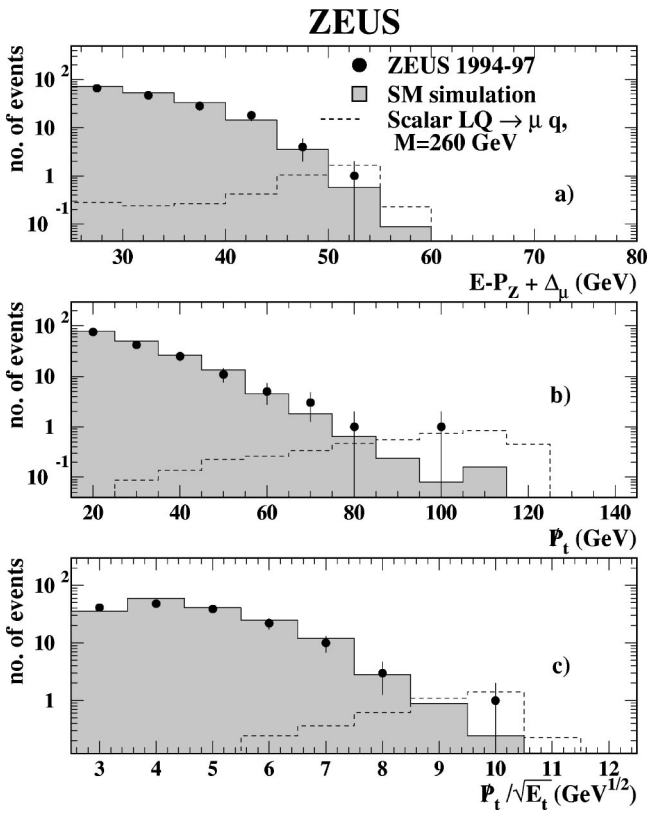

FIG. 2. Distributions of event variables after the μ-channel preselection for data (solid points) and SM simulation (shaded histograms) for (a) $E-P_Z+\Delta_\mu$, (b) $\not{P}_t$, and (c) $\not{P}_t/\sqrt{E_t}$. The dashed histograms simulate the signal from a scalar LQ with $M_{\mathrm{LQ}}=260$ GeV normalized to the 95% C.L. cross-section upper limit (see Sec. IX).

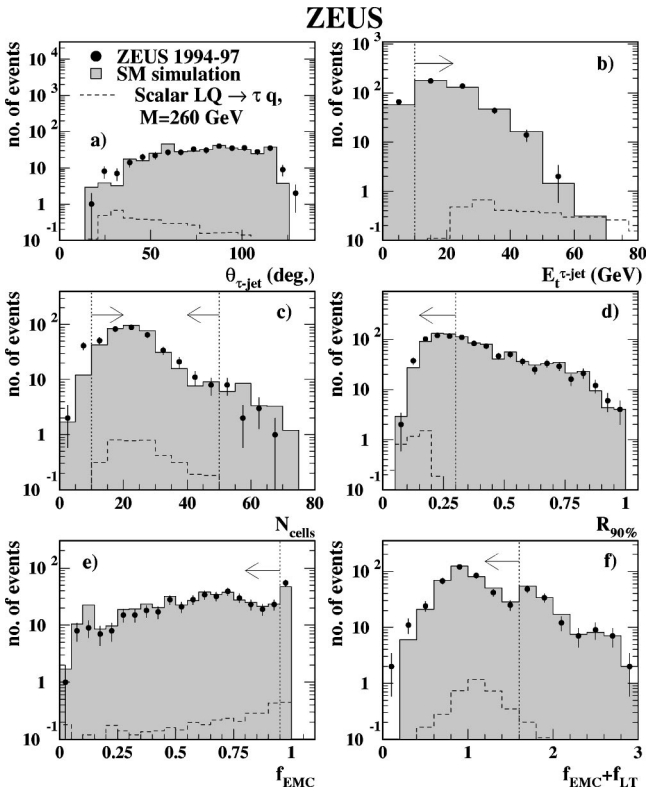

FIG. 3. Comparison of data (solid points) and simulated SM background (shaded histograms) for candidate jets from hadronic τ decays. The distributions are displayed for events that pass the selection cuts described in Sec. VII B except the ones imposed on the variable considered (indicated by the arrows). Shown are the distributions of (a) $\theta_{\tau-\mathrm{jet}}$, the polar angle of the τ candidate jet; (b) $E_t^{\tau-\mathrm{jet}}$, the transverse energy; (c) N_{cells}, the number of calorimeter cells belonging to the jet; (d) $R_{90\%}$, the (η,ϕ) radius containing 90% of the jet energy; (e) f_{EMC}, the fraction of the jet energy in the EMC section of the calorimeter; (f) $f_{\mathrm{EMC}}+f_{\mathrm{LT}}$, where f_{LT} is the momentum of the leading track divided by the jet energy. The SM backgrounds include NC and CC DIS, photoproduction, *W* production, and $\gamma\gamma\rightarrow\tau^+\tau^-$. The dashed histograms simulate the signal from a scalar LQ with a mass of 260 GeV normalized to the 95% C.L. upper limit on the cross section (see Sec. IX).

There are ten different LQ states in the BRW model, four of which can couple to both left- and right-handed leptons. Because of the third assumption above, models in which these states have left- or right-handed couplings will be treated separately in this analysis. Each state is characterized by spin $J=0$ or 1, weak isospin $T=0$, $\frac{1}{2}$, or 1, and fermion number $F=0$ or ±2 (where $F=3B+L$). Following the Aachen notation [12], scalar ($J=0$) and vector ($J=1$) LQs are denoted S_T^χ and V_T^χ, respectively, where $\chi=L$, R denotes the chirality of the lepton that couples to the LQ. When two different hypercharge states are allowed, one is distinguished by a tilde. In this paper, LQs with couplings λ_{eq_α} to an

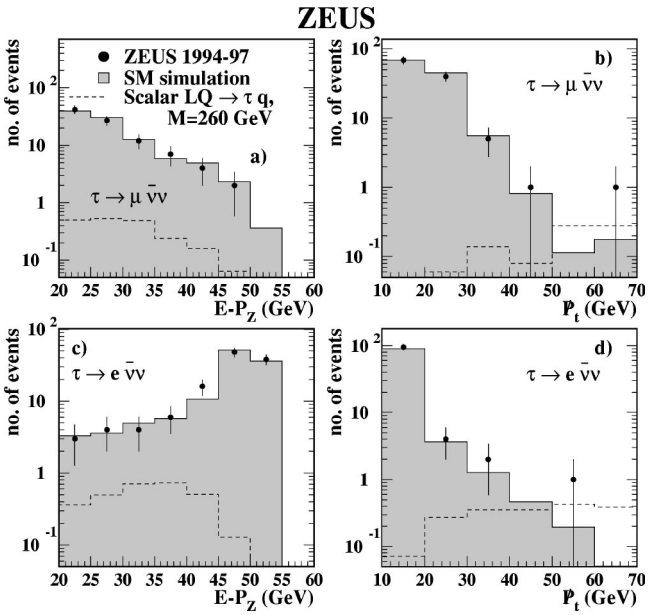

FIG. 4. Comparison of data (solid dots) with simulated SM background (shaded histogram) for the distributions of (a) $E-P_Z$ and (b) $\not{P}_t$ for the $\tau\to\mu\bar{\nu}\nu$ selection. The same distributions for the $\tau\to e\bar{\nu}\nu$ selection are shown in (c) and (d), respectively. The SM backgrounds include NC DIS, photoproduction, CC DIS, W production, and $\gamma\gamma\to\tau^+\tau^-$. The dashed histograms simulate the signal from a scalar LQ with a mass of 260 GeV normalized to the 95% C.L. upper limit on the cross section (see Sec. IX).

electron and a quark q_α, and λ_{lq_β} to a lepton l (μ or τ) and a quark q_β, are considered.[1] The subscripts α and β label the quark generations. The LQ species determines whether q_α or q_β are up- and/or down-type quarks, as shown in the first row of Tables I–IV. In addition to mediating LFV interactions, such LQs would also mediate flavor-conserving interactions with an e or a ν_e in the final state. These final states were not searched for in this analysis, but they were taken into account in calculating branching ratios (the same is true for final states with ν_μ or ν_τ).

In ep collisions, if the LQ mass, $M_{\rm LQ}$, is below $\sqrt{s}$ (low-mass LQs), the LQ is predominantly produced as an s-channel resonance, as shown in Fig. 1(a). In this case, only incident u or d quarks, denoted q_1, that couple to the incident positron to produce $F=0$ LQs, are considered. In the e^+p data analyzed here, the production cross section for $F=0$ LQs is much larger than for $F=-2$ LQs, assuming that $M_{\rm LQ}$ is sufficiently large so that the production is valence-quark dominated, since $F=-2$ LQs would be produced via $e^+\bar{q}$ fusion.

For small values of the Yukawa coupling, λ_{eq1}, the resonance width becomes negligible and the s-channel Breit-Wigner line shape can be approximated (neglecting radiative

[1]Note that in the BRW model, some $\chi=L$ LQs also have neutrino-quark couplings; these couplings are fixed by an $SU(2)_L$ invariance to be equal to the corresponding charged lepton-quark couplings.

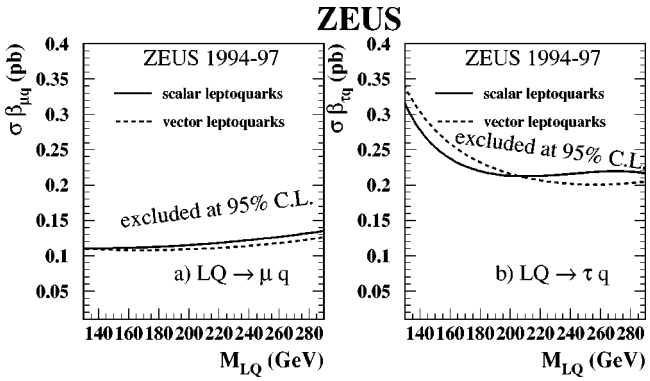

FIG. 5. The 95% C.L. upper limits on $\sigma\beta_{lq}$ as a function of $M_{\rm LQ}$ for scalar (full line) and vector (dashed line) LQs for (a) LQ $\to\mu q$ and (b) LQ$\to\tau q$.

effects) by a δ function at $M_{\rm LQ}=\sqrt{xs}$, where x is the Bjorken variable in deep inelastic scattering (DIS). This leads to the narrow width approximation (NWA)

$$\sigma_{T_3}^{\rm NWA}(s,M_{\rm LQ})=(J+1)\,\frac{\pi\lambda_{eq_1}^2}{4s}\,C_{T_3}q_1\left(x=\frac{M_{\rm LQ}^2}{s},Q_0^2\right), \tag{1}$$

where T_3 is the third component of the weak isospin, C_{T_3} is the square of the relevant SU(2) Clebsch-Gordan coefficient,

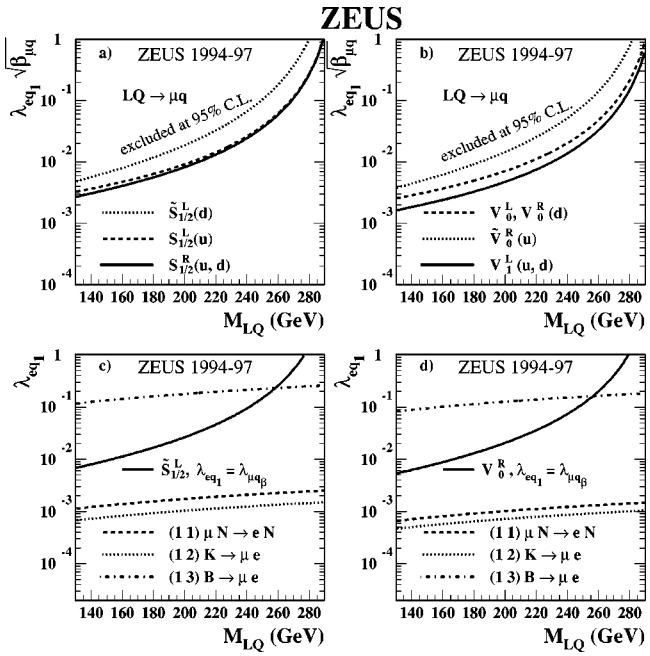

FIG. 6. Upper limits on $\lambda_{eq_1}\sqrt{\beta_{\mu q}}$ vs $M_{\rm LQ}$ for (a) scalar and (b) vector LQs. The quark flavors that couple to the LQs in the initial state are shown in parentheses following the LQ species. Upper limits on λ_{eq_1} under the assumption $\beta_{\mu q}=0.5$ are shown in (c) for scalar LQs and (d) for vector LQs that couple to d-type quarks. Also shown are existing limits [8,43,44] (dashed lines). The numbers in parentheses indicate the generations of the quarks that couple to the e and the μ, respectively. The regions above the curves are excluded at the 95% C.L.

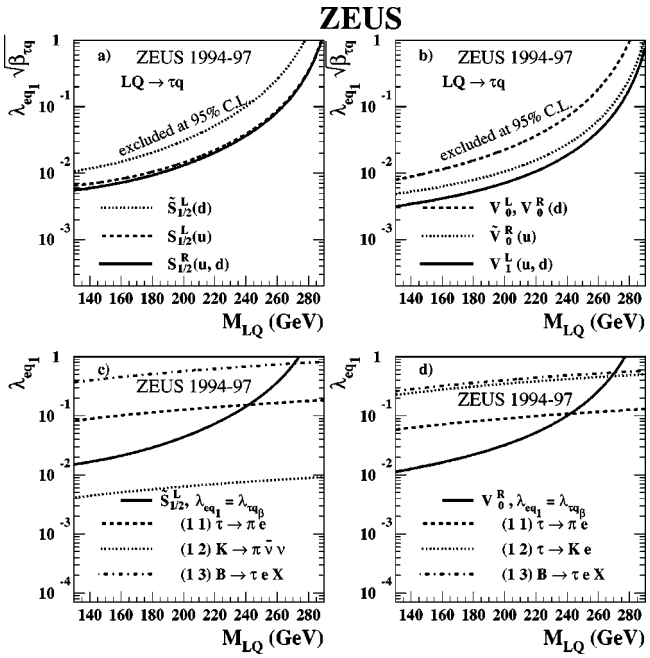

FIG. 7. Upper limits on $\lambda_{eq_1}\sqrt{\beta_{\tau q}}$ vs M_{LQ} for (a) scalar and (b) vector LQs. The quark flavors that couple to the LQs in the initial state are shown in parentheses following the LQ species. Upper limits on λ_{eq_1} under the assumption $\beta_{\tau q}=0.5$ are shown in (c) for scalar LQs and (d) for vector LQs that couple to *d*-type quarks. Also shown are existing limits [8,43,44] (dashed lines). The numbers in parentheses indicate the generations of the quarks that couple to the *e* and the τ, respectively. The regions above the curves are excluded at the 95% C.L.

and $q_1(x,Q_0^2)$ is the valence-quark density in the proton evaluated at the scale $Q_0^2=M_{\mathrm{LQ}}^2$. The total production cross section for a given LQ is given by the sum over all states of the SU(2) multiplet that couple to a positron and a quark. The NWA becomes inaccurate if $q_1(x,Q_0^2)$ varies significantly with x on a scale corresponding to the LQ width, $\Gamma_{\mathrm{LQ}}\propto\lambda^2 M_{\mathrm{LQ}}$. In the present analysis, this occurs only when M_{LQ} is close to $\sqrt{s}(x\rightarrow 1)$. In this region, q_1 falls steeply with x and the convolution of q_1 with the Breit-Wigner lineshape results in contributions to the cross section from quarks with x below the resonant peak. These nonresonant contributions to the cross section are neglected in the NWA. For LQs that couple to u (d) quarks, with $M_{\mathrm{LQ}}=270$ GeV (250 GeV) and $\lambda_{eq_1}=0.3$, σ^{NWA} underestimates the cross section by $\simeq$20%. The rate for LFV events is proportional to $\sigma\beta_{lq}$ where β_{lq} is the branching ratio to the lq final state. In this paper, the NWA is used to calculate cross sections for $M_{\mathrm{LQ}}<\sqrt{s}$, so that limits on $\sigma\beta_{lq}$ can be simply converted to limits on $\lambda_{eq_1}\sqrt{\beta_{lq}}$. The NWA underestimates the cross section, leading to conservative limits.

If $M_{\mathrm{LQ}}>\sqrt{s}$ (high-mass LQs), both *s*- and *u*-channel diagrams contribute, see Fig. 1. If $M_{\mathrm{LQ}}\gg\sqrt{s}$, the LQ propagator contracts to a four-fermion contact interaction and the cross section is proportional to $[\lambda_{eq_\alpha}\lambda_{lq_\beta}/M_{\mathrm{LQ}}^2]^2$. In this high-mass approximation (HMA), the cross section for an $F=0$ LQ, in e^+p collisions, can be written as

$$\sigma_{F=0}^{HMA}=\frac{s}{32\pi}\left[\frac{\lambda_{eq_\alpha}\lambda_{lq_\beta}}{M_{\mathrm{LQ}}^2}\right]^2\left[\int dx\,dy\,xq_\alpha(x,\hat{s})f(y)+\int dx\,dy\,x\overline{q}_\beta(x,-\hat{u})g(y)\right], \tag{2}$$

with

$$f(y)=\begin{cases}1/2 & \text{scalar LQ}\\ 2(1-y)^2 & \text{vector LQ,}\end{cases}$$

$$g(y)=\begin{cases}(1-y)^2/2 & \text{scalar LQ}\\ 2 & \text{vector LQ,}\end{cases}$$

where y is the inelasticity, $\hat{s}=sx$ and $\hat{u}=sx(y-1)$ are the scales at which the quark densities q_α and $\overline{q}_\beta$ are evaluated. The first and second integrals in Eq. (2) are due to the *s*- and *u*-channel contributions, respectively ($|F|=2$ LQs couple a quark in the *u*-channel and an antiquark in the *s* channel). The accuracy of the HMA increases with increasing LQ mass. For $M_{\mathrm{LQ}}>600$ GeV, the minimum mass considered for this high-mass analysis, the accuracy is better than 10%. In the high-mass case, LQ scenarios are characterized by the 14 LQ species, the three generations of q_α and q_β, and the two possible final-state leptons, leading to a total of 252 different LQ scenarios.

NLO QCD corrections [13,14] were applied only to the NWA production cross section for scalar LQs, since no calculation is available for vector LQs or for high-mass scalar LQs. These corrections increase the production cross section by $\simeq$15% at $M_{\mathrm{LQ}}=150$ GeV, increasing to $\simeq$30% at $M_{\mathrm{LQ}}=250$ GeV.

Corrections for QED initial-state radiation (ISR), evaluated using the Weizsäcker-Williams approximation [15,16], were applied to both the low- and high-mass cases. The QED ISR correction reduces the NWA cross section by $\sim$3% at $M_{\mathrm{LQ}}=150$ GeV and by $\sim$25% when M_{LQ} approaches the kinematic limit. For high-mass LQs, QED ISR corrections, evaluated at $M_{\mathrm{LQ}}=600$ GeV, were applied. They lower the cross section by less than 5%; the corrections decrease at higher masses.

B. *R*-parity-violating squarks

Supersymmetry (SUSY), which links bosons and fermions, is a promising extension to the SM. It assumes a supersymmetric partner for each SM particle, a bosonic partner for a fermion, and vice versa. R parity is a multiplicative quantum number defined as $R_p=(-1)^{3B+L+2J}$. For SM particles, $R_p=1$; for SUSY particles (sparticles), $R_p=-1$. In R_p-conserving processes, sparticles are pair produced and the lightest supersymmetric particle (LSP) is stable. In models with R_p violation ($\not{R}_p$), single SUSY-particle production is

TABLE I. Upper limits at 95% C.L. on $\lambda_{eq\alpha}\lambda_{\mu q\beta}/M^2_{\mathrm{LQ}}$ in units of TeV^{-2} for $F=0$ LQs that couple to eq_α and to μq_β. The columns correspond to the $F=0$ LQ species. The eq_α combination for the s-channel case is reported under the LQ type. Each row corresponds to a different combination of quark generations (α, β) which couple to the position and the μ, respectively. Within each cell, the measurement providing the most stringent low-energy constraint is shown on the first line and the corresponding limit [8,43,44] is given on the second line. The ZEUS limits are shown on the third line of each cell (identified by an underline when stronger than the low-energy constraint). The $*$ indicates cases where a top quark must be involved.

	$e\to\mu$		ZEUS		$F=0$		
$\alpha\beta$	$\mathbf{S^L_{1/2}}$ e^+u_α	$\mathbf{S^R_{1/2}}$ $e^+(u+d)_\alpha$	$\mathbf{\tilde{S}^L_{1/2}}$ e^+d_α	$\mathbf{V^L_0}$ e^+d_α	$\mathbf{V^R_0}$ e^+d_α	$\mathbf{\tilde{V}^R_0}$ e^+u_α	$\mathbf{V^L_1}$ $e^+(\sqrt{2}u+d)_\alpha$
1 1	**μN→eN** 7.6×10^{-5} **1.9**	**μN→eN** 2.6×10^{-5} **1.6**	**μN→eN** 7.6×10^{-5} **2.9**	**μN→eN** 2.6×10^{-5} **1.9**	**μN→eN** 2.6×10^{-5} **1.9**	**μN→eN** 2.6×10^{-5} **1.5**	**μN→eN** 1.1×10^{-5} **0.7**
1 2	**D→$\mu\bar{e}$** 4 **1.9**	**K→$\mu\bar{e}$** 2.7×10^{-5} **1.6**	**K→$\mu\bar{e}$** 2.7×10^{-5} **3.0**	**K→$\mu\bar{e}$** 1.3×10^{-5} **2.3**	**K→$\mu\bar{e}$** 1.3×10^{-5} **2.3**	**D→$\mu\bar{e}$** 2 **1.7**	**K→$\mu\bar{e}$** 1.3×10^{-5} **0.8**
1 3	*	**B→$\mu\bar{e}$** 0.8 **3.1**	**B→$\mu\bar{e}$** 0.8 **3.1**	$\mathbf{V_{ub}}$ 0.2 **2.7**	**B→$\mu\bar{e}$** 0.4 **2.7**	*	$\mathbf{V_{ub}}$ 0.2 **2.7**
2 1	**D→$\mu\bar{e}$** 4 **8.5**	**K→$\mu\bar{e}$** 2.7×10^{-5} **4.9**	**K→$\mu\bar{e}$** 2.7×10^{-5} **6.2**	**K→$\mu\bar{e}$** 1.3×10^{-5} **2.8**	**K→$\mu\bar{e}$** 1.3×10^{-5} **2.8**	**D→$\mu\bar{e}$** 2 **3.2**	**K→$\mu\bar{e}$** 1.3×10^{-5} **1.5**
2 2	**μ→ee$\bar{e}$** 5×10^{-3} **11**	**μ→eee** 7.3×10^{-3} **5.5**	**μ→ee$\bar{e}$** 1.6×10^{-2} **6.9**	**μ→ee$\bar{e}$** 8×10^{-3} **3.4**	**μ→ee$\bar{e}$** 8×10^{-3} **3.4**	**μ→ee$\bar{e}$** 2.5×10^{-3} **5.1**	**μ→ee$\bar{e}$** 1.5×10^{-3} **2.2**
2 3	*	**B→$\bar{\mu}$eK** 0.6 **8.8**	**B→$\bar{\mu}eK$** 0.6 **8.8**	**B→$\bar{\mu}$eK** 0.3 **5.7**	**B→$\bar{\mu}$eK** 0.3 **5.7**	*	**B→$\bar{\mu}$eK** 0.3 **5.7**
3 1	*	**B→$\mu\bar{e}$** 0.8 **9.3**	**B→$\mu\bar{e}$** 0.8 **9.3**	$\mathbf{V_{ub}}$ 0.2 **3.2**	**B→$\mu\bar{e}$** 0.4 **3.2**	*	$\mathbf{V_{ub}}$ 0.2 **3.2**
3 2	*	**B→$\bar{\mu}$eK** 0.6 **11**	**B→$\bar{\mu}$eK** 0.6 **11**	**B→$\bar{\mu}$eK** 0.3 **3.9**	**B→$\bar{\mu}$eK** 0.3 **3.9**	*	**B→$\bar{\mu}$eK** 0.3 **3.9**
3 3	*	**μ→ee$\bar{e}$** 7.3×10^{-3} **16**	**μ→ee$\bar{e}$** 1.6×10^{-2} **16**	**μ→ee$\bar{e}$** 8×10^{-3} **8.0**	**μ→ee$\bar{e}$** 8×10^{-3} **8.0**	*	**μ→ee$\bar{e}$** 1.5×10^{-3} **8.0**

possible and the LSP decays into SM particles. Of special interest for HERA are $\not{R}_p$ Yukawa couplings that couple a squark (SUSY partner of a quark) to a lepton and a quark, which are described in the superpotential by the term [17] $\lambda'_{ijk}L^iQ^j\bar{D}^k$, where i, j, and k are generation indices, L and Q denote the left-handed lepton and quark-doublet superfields, respectively, and $\bar{D}$ denotes the right-handed quark-singlet chiral superfield. Expansion of the superfields using four-component Dirac notation yields

$$\mathcal{L}=\lambda'_{ijk}[-\tilde{e}^i_L u^j_L \bar{d}^k_R - e^i_L \tilde{u}^j_L \bar{d}^k_R - (\bar{e^i_L})^c u^j_L (\tilde{d}^k_R)^* + \tilde{\nu}^i_L d^j_L \bar{d}^k_R + \nu^i_L \tilde{d}^j_L \bar{d}^k_R + (\bar{\nu^i_L})^c d^j_L (\tilde{d}^k_R)^*] + \text{H.c.} \quad (3)$$

The superscript c denotes charge conjugation and the asterisk denotes complex conjugation of scalar fields. For $i=1$, the second and third terms will result in $\tilde{u}^j$ and $\tilde{d}^k$ production in ep collisions. Identical terms appear in the Lagrangians for the scalar leptoquarks $\tilde{S}^L_{1/2}$ and S^L_0 [18]. The coupling λ'_{1j1} gives rise to the reaction $e^+d\to\tilde{u}^j_L$, while the coupling λ'_{11k} would cause the reaction $e^-u\to\tilde{d}^k_R$.

Lepton-flavor violation would occur in models with two nonzero Yukawa couplings involving different lepton generations. For example, nonzero values of λ'_{1j1} and λ'_{ijk} ($i=2,3$) would yield the process $e^+d\to\tilde{u}^j\to l^+d^k$, where $i=2,\ 3$ corresponds to $l=\mu,\ \tau$. Squarks also undergo R_p-conserving decays to a quark and a gaugino, which were not considered in this analysis. Low-mass coupling limits on

TABLE II. Upper limits at 95% C.L. on $\lambda_{eq\alpha}\lambda_{eq\beta}/M_{\mathrm{LQ}}^2$ in units of TeV^{-2} for $|F|=2$ LQs that couple to eq_α and to μq_β. The columns correspond to the $|F|=2$ LQ species. The format of the table is described in the caption of Table I.

	$e\to\mu$		ZEUS		$\lvert F\rvert=2$		
$\alpha\beta$	$\mathbf{S_0^L}$ $e^+\bar{u}_\alpha$	$\mathbf{S_0^R}$ $e^+\bar{u}_\alpha$	$\mathbf{\tilde{S}_0^R}$ $e^+\bar{d}_\alpha$	$\mathbf{S_1^L}$ $e^+(\bar{u}+\sqrt{2}\bar{d})_\alpha$	$\mathbf{V_{1/2}^L}$ $e^+\bar{d}_\alpha$	$\mathbf{\tilde{V}_{1/2}^R}$ $e^+(\bar{u}+\bar{d})_\alpha$	$\mathbf{\tilde{V}_{1/2}^L}$ $e^+\bar{u}_\alpha$
	$\boldsymbol{\mu}\mathbf{N}\to\mathbf{eN}$	$\boldsymbol{\mu}\mathbf{N}\to\mathbf{eN}$	$\boldsymbol{\mu}\mathbf{N}\to\mathbf{eN}$	$\boldsymbol{\mu}\mathbf{N}\to\mathbf{eN}$	$\boldsymbol{\mu}\mathbf{N}\to\mathbf{eN}$	$\boldsymbol{\mu}\mathbf{N}\to\mathbf{eN}$	$\boldsymbol{\mu}\mathbf{N}\to\mathbf{eN}$
1 1	7.6×10^{-5}	7.6×10^{-5}	7.6×10^{-5}	2.3×10^{-5}	2.6×10^{-5}	1.3×10^{-5}	2.6×10^{-5}
	3.4	**3.4**	**4.2**	**1.8**	**1.5**	**0.8**	**1.0**
	$\mathbf{K}\to\boldsymbol{\pi\nu\bar{\nu}}$	$\mathbf{D}\to\boldsymbol{\mu\bar{e}}$	$\mathbf{K}\to\boldsymbol{\mu\bar{e}}$	$\mathbf{K}\to\boldsymbol{\mu\bar{e}}$	$\mathbf{K}\to\boldsymbol{\mu\bar{e}}$	$\mathbf{K}\to\boldsymbol{\mu\bar{e}}$	$\mathbf{D}\to\boldsymbol{\mu\bar{e}}$
1 2	10^{-3}	4	2.7×10^{-5}	1.3×10^{-5}	1.3×10^{-5}	1.3×10^{-5}	2
	7.1	**7.1**	**5.6**	**2.6**	**3.1**	**2.5**	**4.4**
	$\mathbf{V}_{ub}$		$\mathbf{B}\to\boldsymbol{\mu\bar{e}}$	$\mathbf{V}_{ub}$	$\mathbf{B}\to\boldsymbol{\mu\bar{e}}$	$\mathbf{B}\to\boldsymbol{\mu\bar{e}}$	
1 3	0.4	*	0.8	0.4	0.4	0.4	*
	*		**6.6**	**3.2**	**4.7**	**4.7**	
	$\mathbf{K}\to\boldsymbol{\pi\nu\bar{\nu}}$	$\mathbf{D}\to\boldsymbol{\mu\bar{e}}$	$\mathbf{K}\to\boldsymbol{\mu\bar{e}}$	$\mathbf{K}\to\boldsymbol{\mu\bar{e}}$	$\mathbf{K}\to\boldsymbol{\mu\bar{e}}$	$\mathbf{K}\to\boldsymbol{\mu\bar{e}}$	$\mathbf{D}\to\boldsymbol{\mu\bar{e}}$
2 1	10^{-3}	4	2.7×10^{-5}	1.3×10^{-5}	1.3×10^{-5}	1.3×10^{-5}	2
	3.7	**3.7**	**4.7**	**2.0**	**1.6**	**0.9**	**1.0**
	$\boldsymbol{\mu}\mathbf{\to ee\bar{e}}$	$\boldsymbol{\mu}\mathbf{\to eee}$	$\boldsymbol{\mu}\mathbf{\to ee\bar{e}}$	$\boldsymbol{\mu}\mathbf{\to ee\bar{e}}$	$\boldsymbol{\mu}\mathbf{\to ee\bar{e}}$	$\boldsymbol{\mu}\mathbf{\to ee\bar{e}}$	$\boldsymbol{\mu}\mathbf{\to ee\bar{e}}$
2 2	5×10^{-3}	5×10^{-3}	1.6×10^{-2}	1.3×10^{-2}	8×10^{-3}	3.7×10^{-3}	2.5×10^{-3}
	11	**11**	**6.9**	**3.4**	**3.4**	**2.8**	**5.1**
	$\mathbf{B}\to\mathbf{l}\boldsymbol{\nu}\mathbf{X}$		$\mathbf{B}\to\boldsymbol{\bar{\mu}}\mathbf{eK}$	$\mathbf{B}\to\boldsymbol{\bar{\mu}}eK$	$\mathbf{B}\to\boldsymbol{\bar{\mu}}\mathbf{eK}$	$\mathbf{B}\to\boldsymbol{\bar{\mu}}\mathbf{eK}$	
2 3	4	*	0.6	0.3	0.3	0.3	*
	*		**8.8**	**4.4**	**5.7**	**5.7**	
	$\mathbf{V}_{ub}$		$\mathbf{B}\to\boldsymbol{\mu\bar{e}}$	$\mathbf{V}_{ub}$	$\mathbf{B}\to\boldsymbol{\mu\bar{e}}$	$\mathbf{B}\to\boldsymbol{\mu\bar{e}}$	
3 1	0.4	*	0.8	0.4	0.4	0.4	*
	*		**5.6**	**2.8**	**1.6**	**1.6**	
	$\mathbf{B}\to\mathbf{l}\boldsymbol{\nu}\mathbf{X}$		$\mathbf{B}\to\boldsymbol{\bar{\mu}}\mathbf{eK}$	$\mathbf{B}\to\boldsymbol{\bar{\mu}}\mathbf{eK}$	$\mathbf{B}\to\boldsymbol{\bar{\mu}}\mathbf{eK}$	$\mathbf{B}\to\boldsymbol{\bar{\mu}}\mathbf{eK}$	
3 2	4	*	0.6	0.3	0.3	0.3	*
	*		**11**	**5.6**	**3.9**	**3.9**	
			$\boldsymbol{\mu}\mathbf{\to ee\bar{e}}$	$\boldsymbol{\mu}\mathbf{\to ee\bar{e}}$	$\boldsymbol{\mu}\mathbf{\to ee\bar{e}}$	$\boldsymbol{\mu}\mathbf{\to ee\bar{e}}$	
3 3	*	*	1.6×10^{-2}	1.3×10^{-2}	8×10^{-3}	3.7×10^{-3}	*
			16	**8.2**	**8.0**	**8.0**	

$\tilde{S}_{1/2}^L$ LQs can be interpreted, using $\lambda_{eq_1}\sqrt{\beta_{lq}}=\lambda'_{1j1}\sqrt{\beta_{\tilde{u}^j\to lq}}$, as limits on $\tilde{u}^j$ squarks that couple to eq_1 and to lq. In the low-mass case, the limits apply for any final-state quark q (except top). High-mass LQ limits can also be applied to squarks as described in Sec. IX C.

III. THE ZEUS DETECTOR

A detailed description of the ZEUS detector can be found elsewhere [19]. A brief outline of the components that are most relevant for this analysis is given below. Charged particles are tracked in the central tracking detector (CTD) [20], which operates in a magnetic field of 1.43 T provided by a thin superconducting coil. The CTD consists of 72 cylindrical drift chamber layers, organized in nine superlayers covering the polar angle[2] region $15°<\theta<164°$. The transverse-momentum resolution for full-length tracks is $\sigma(p_T)/p_T=0.0058p_T\oplus0.0065\oplus0.0014/p_T$, with p_T in GeV. The CTD was used to reconstruct tracks of isolated muons and charged τ-decay products. It was also used to determine the interaction vertex with a typical resolution of 4 mm (1 mm) along (transverse to) the beam direction.

[2]The ZEUS coordinate system is a right-handed Cartesian system with the Z axis pointing in the proton beam direction, referred to as the "forward direction," and the X axis pointing left towards the center of HERA. The coordinate origin is at the nominal interaction point. The pseudorapidity is defined as $\eta=-\ln[\tan(\theta/2)]$, where the polar angle θ is measured with respect to the proton beam direction.

TABLE III. Upper limits at 95% C.L. on $\lambda_{eq\alpha}\lambda_{\tau\omega\beta}/M_{\mathrm{LQ}}^2$ in units of TeV^{-2} for $F=2$ LQs that couple to eq_α and to τq_β. The columns correspond to the $F=2$ LQ species. The format of the table is described in the caption of Table I.

	$e\to\tau$		ZEUS		$F=0$		
$\alpha\beta$	$\mathbf{S_{1/2}^L}$ e^+u_α	$\mathbf{S_{1/2}^R}$ $e^+(u+d)_\alpha$	$\mathbf{\tilde{S}_{1/2}^L}$ e^+d_α	$\mathbf{V_0^L}$ e^+d_α	$\mathbf{V_0^R}$ e^+d_α	$\mathbf{\tilde{V}_0^R}$ e^+u_α	$\mathbf{V_1^L}$ $e^+(\sqrt{2}u+d)_\alpha$
	$\boldsymbol{\tau\to\pi e}$	$\boldsymbol{\tau\to\pi e}$	$\boldsymbol{\tau\to\pi e}$	$\mathbf{G_F}$	$\boldsymbol{\tau\to\pi e}$	$\boldsymbol{\tau\to\pi e}$	$\mathbf{G_F}$
1 1	0.4	0.2	0.4	0.2	0.2	0.2	0.2
	3.0	**2.5**	**4.6**	**3.3**	**3.3**	**2.4**	**1.2**
		$\boldsymbol{\tau\to Ke}$	$\mathbf{K\to\pi\nu\bar{\nu}}$	$\boldsymbol{\tau\to Ke}$	$\boldsymbol{\tau\to Ke}$		$\mathbf{K\to\pi\nu\bar{\nu}}$
1 2		5	10^{-3}	3	3		2.5×10^{-4}
	3.1	**2.5**	**4.7**	**3.7**	**3.7**	**2.7**	**1.3**
		$\mathbf{B\to\pi\bar{e}X}$	$\mathbf{B\to\pi\bar{e}X}$	$\mathbf{B\to l\nu X}$	$\mathbf{B\to\pi\bar{e}X}$		$\mathbf{B\to l\nu X}$
1 3	*	8	8	2	4	*	2
		5.1	**5.1**	**4.6**	**4.6**		**4.6**
		$\boldsymbol{\tau\to Ke}$	$\mathbf{K\to\pi\nu\bar{\nu}}$	$\boldsymbol{\tau\to Ke}$	$\boldsymbol{\tau\to Ke}$		$\mathbf{K\to\pi\nu\bar{\nu}}$
2 1		5	10^{-3}	3	3		2.5×10^{-4}
	16	**9.2**	**12**	**4.9**	**4.9**	**6.2**	**2.6**
	$\boldsymbol{\tau\to ee\bar{e}}$	$\boldsymbol{\tau\to ee\bar{e}}$	$\boldsymbol{\tau\to ee\bar{e}}$	$\boldsymbol{\tau\to ee\bar{e}}$	$\boldsymbol{\tau\to ee\bar{e}}$	$\boldsymbol{\tau\to ee\bar{e}}$	$\boldsymbol{\tau\to ee\bar{e}}$
2 2	20	30	66	33	33	10	6.1
	20	**11**	**12**	**6.2**	**6.2**	**11**	**4.3**
		$\mathbf{B\to\pi\bar{e}X}$	$\mathbf{B\to\pi\bar{e}X}$	$\mathbf{B\to l\nu X}$	$\mathbf{B\to\pi\bar{e}X}$		$\mathbf{B\to l\nu X}$
2 3	*	8	8	2	4	*	2
		16	**16**	**12**	**12**		**12**
		$\mathbf{B\to\pi\bar{e}X}$	$\mathbf{B\to\pi\bar{e}X}$	$\mathbf{V_{ub}}$	$\mathbf{B\to\pi\bar{e}X}$		$\mathbf{V_{ub}}$
3 1	*	8	8	0.2	4	*	0.2
		17	**17**	**5.4**	**5.4**		**5.4**
		$\mathbf{B\to\pi\bar{e}X}$	$\mathbf{B\to\pi\bar{e}X}$	$\mathbf{B\to l\nu X}$	$\mathbf{B\to\pi\bar{e}X}$		$\mathbf{B\to l\nu X}$
3 2	*	8	8	2	4	*	2
		22	**22**	**7.6**	**7.6**		**7.6**
		$\boldsymbol{\tau\to ee\bar{e}}$	$\boldsymbol{\tau\to ee\bar{e}}$	$\boldsymbol{\tau\to ee\bar{e}}$	$\boldsymbol{\tau\to ee\bar{e}}$		$\boldsymbol{\tau\to ee\bar{e}}$
3 3	*	30	66	33	33	*	6.1
		30	**30**	**15**	**15**		**15**

The high-resolution uranium-scintillator calorimeter (CAL) [21] consists of three parts: the forward (FCAL), the barrel (BCAL), and the rear (RCAL) calorimeters. The calorimeters are subdivided into towers, each of which subtends a solid angle from 0.006 to 0.04 steradians. Each tower is longitudinally segmented into an electromagnetic (EMC) section and two hardronic (HAC) sections (one in RCAL). Each HAC section consists of a single cell, while the EMC section of each tower is further subdivided transversely into four cells (two in RCAL). The CAL energy resolutions, as measured under test-beam conditions, are $\sigma(E)/E=0.18/\sqrt{E}$ for electrons and $\sigma(E)/E=0.35/\sqrt{E}$ for hadrons (E in GeV). The arrival time of CAL energy deposits is measured with subnanosecond resolution for energy deposits above 4.5 GeV, allowing the rejection of non-ep background.

The FMUON detector [19] consists of layers of limited streamer tubes and drift-chamber planes located up to 10 m from the interaction point. The toroidal magnetic fields of the iron yoke (1.4 T) that surrounds the CAL and of two toroids (1.6 T) located about 9 m from the interaction point enable muon momentum measurements to be made. The FMUON tags high-momentum muons (muons with momenta below 5 GeV are unlikely to emerge from the FCAL) with polar angles in the range $8°<\theta<20°$, extending well beyond the CTD acceptance.

The luminosity was measured by the luminosity detector (LUMI) from the rate of the Bethe-Heitler process $e^+p\to e^+\gamma p$ [22], where the photon is detected in a lead-scintillator calorimeter located at $Z=-107$ m in the HERA tunnel. The uncertainty on the luminosity measurement was 1.6%.

IV. MONTE CARLO SIMULATION

The simulation of the LQ signal, including both s- and u-channel processes, was performed using the generators

TABLE IV. Upper limits at 95% C.L. on $\lambda_{eq\alpha}\lambda_{\tau\omega\beta}/M^2_{\mathrm{LQ}}$ in units of TeV^{-2} for $|F|=2$ LQs that couple to eq_α and to τq_β. The columns correspond to the $|F|=2$ LQ species. The format of the table is described in the caption of Table I.

	$e\to\tau$		ZEUS		$\lvert F\rvert=2$		
$\alpha\beta$	$\mathbf{S_0^L}$ $e^+\bar{u}_\alpha$	$\mathbf{S_0^R}$ $e^+\bar{u}_\alpha$	$\mathbf{\tilde{S}_0^R}$ $e^+\bar{d}_\alpha$	$\mathbf{S_1^L}$ $e^+(\bar{u}+\sqrt{2}\bar{d})_\alpha$	$\mathbf{V_{1/2}^L}$ $e^+\bar{d}_\alpha$	$\mathbf{V_{1/2}^R}$ $e^+(\bar{u}+\bar{d})_\alpha$	$\mathbf{\tilde{V}_{1/2}^L}$ $e^+\bar{u}_\alpha$
	$\mathbf{G_F}$	$\boldsymbol{\tau\to\pi e}$	$\boldsymbol{\tau\to\pi e}$	$\mathbf{G_F}$	$\boldsymbol{\tau\to\pi e}$	$\boldsymbol{\tau\to\pi e}$	$\boldsymbol{\tau\to\pi e}$
1 1	0.3	0.4	0.4	0.3	0.2	0.1	0.2
	5.4	**5.4**	**7.1**	**2.8**	**2.6**	**1.3**	**1.7**
	$\mathbf{K\to\pi\nu\bar{\nu}}$		$\boldsymbol{\tau\to}$**Ke**	$\mathbf{K\to\pi\nu\bar{\nu}}$	$\mathbf{K\to\pi\nu\bar{\nu}}$	$\boldsymbol{\tau\to}$**Ke**	
1 2	10^{-3}		5	10^{-3}	5×10^{-4}	3	
	14	**14**	**9.3**	**4.6**	**5.5**	**4.5**	**8.2**
	$\mathbf{V_{ub}}$		$\mathbf{B\to\pi\bar{e}X}$	$\mathbf{V_{ub}}$	$\mathbf{B\to\pi\bar{e}X}$	$\mathbf{B\to\pi\bar{e}X}$	
1 3	0.4	*	8	0.4	4	4	*
	*		**12**	**5.5**	**8.4**	**8.4**	
	$\mathbf{K\to\pi\nu\bar{\nu}}$		$\boldsymbol{\tau\to}$**Ke**	$\mathbf{K\to\pi\nu\bar{\nu}}$	$\mathbf{K\to\pi\nu\bar{\nu}}$	$\boldsymbol{\tau\to}$**Ke**	
2 1	10^{-3}		5	10^{-3}	5×10^{-4}	3	
	5.9	**5.9**	**7.8**	**3.2**	**2.5**	**1.3**	**1.6**
	$\boldsymbol{\tau\to e\bar{e}e}$	$\boldsymbol{\tau\to e\bar{e}e}$	$\boldsymbol{\tau\to e\bar{e}e}$	$\boldsymbol{\tau\to e\bar{e}e}$	$\boldsymbol{\tau\to e\bar{e}e}$	$\boldsymbol{\tau\to e\bar{e}e}$	$\boldsymbol{\tau\to e\bar{e}e}$
2 2	20	20	66	55	33	15	10
	19	**19**	**13**	**6.2**	**6.5**	**5.2**	**9.7**
	$\mathbf{B\to l\nu X}$		$\mathbf{B\to\pi\bar{e}X}$	$\mathbf{B\to l\nu X}$	$\mathbf{B\to\pi\bar{e}X}$	$\mathbf{B\to\pi\bar{e}X}$	
2 3	4	*	8	4	4	4	*
	*		**17**	**8.1**	**11**	**11**	
	$\mathbf{B\to l\nu X}$		$\mathbf{B\to\pi\bar{e}X}$	$\mathbf{B\to l\nu X}$	$\mathbf{B\to\pi\bar{e}X}$	$\mathbf{B\to\pi\bar{e}X}$	
3 1	4	*	8	4	4	4	*
	*		**9.3**	**4.7**	**2.6**	**2.6**	
	$\mathbf{B\to l\nu X}$		$\mathbf{B\to\pi\bar{e}X}$	$\mathbf{B\to l\nu X}$	$\mathbf{B\to\pi\bar{e}X}$	$\mathbf{B\to\pi\bar{e}X}$	
3 2	4	*	8	4	4	4	*
	*		**21**	**10.2**	**7.6**	**7.6**	
			$\boldsymbol{\tau\to e\bar{e}e}$	$\boldsymbol{\tau\to e\bar{e}e}$	$\boldsymbol{\tau\to e\bar{e}e}$	$\boldsymbol{\tau\to e\bar{e}e}$	
3 3	*	*	66	55	33	15	*
			30	**16**	**15**	**15**	

LQMGEN 1.0 [23] (low-mass LQs) and LQGENEP 1.0 [24] (high-mass LQs) based on the BRW model [11]. Both generators are interfaced to JETSET 7.4 [25] to simulate hadronization and particle decays.

The following SM backgrounds were considered: charged current (CC) and neutral current (NC) deep inelastic scattering (DIS) were simulated using DJANGO6 2.4 [26], with the color-dipole model ARIADNE 4.08 [27] used to simulate the hadronic final state. Elastic and inelastic $\gamma\gamma\to l^+l^-$ reactions were simulated with LPAIR [28]. EPVEC 1.0 [29] was used to simulate W production. Photoproduction processes were simulated with HERWIG 5.8 [30]. The ZEUS detector and trigger were simulated with a program based on GEANT 3.13 [31]. The simulated events were processed by the same reconstruction programs as the data.

V. KINEMATIC QUANTITIES

Global calorimeter sums were calculated as follows: each calorimeter cell i with an energy deposit E_i above a threshold was assigned a four-momentum P^μ, defined as $P^\mu=(E_i,E_i\cos\phi_i\sin\theta_i,E_i\sin\phi_i\sin\theta_i,E_i\cos\theta_i)$, where ϕ_i and θ_i are the azimuthal and polar angles of the cell center relative to the event vertex. The total four-momentum deposited in the calorimeter (E,P_X,P_Y,P_Z) is given by the sum of the four-momenta for all cells. The transverse energy, E_t, is given by $\Sigma_i E_i\sin\theta_i$. The missing transverse momentum $\not{P}_t$ is given by $\sqrt{P_X^2+P_Y^2}$. The azimuth assigned to $\not{P}_t,\phi_{\mathrm{miss}}$, was defined by $\cos\phi_{\mathrm{miss}}=-P_X/\not{P}_t$ and $\sin\phi_{\mathrm{miss}}=-P_Y/\not{P}_t$. Jets used in identifying hadronic τ decays were reconstructed using an (η,ϕ) cone algorithm [32] with cone

TABLE V. The 95% C.L. lower limits on M_{LQ} for the μ and the τ channels assuming $\lambda_{eq_1}=\lambda_{lq}=0.3$.

LQ type	$\tilde{S}^L_{1/2}$	$S^L_{1/2}$	$S^R_{1/2}$	V^L_0	V^R_0	$\tilde{V}_0 R$	V^L_1
μ-channel limit on M_{LQ} (GeV)	263	278	278	261	266	280	283
τ-channel limit on M_{LQ} (GeV)	258	275	276	259	263	277	282

radius $R=1$. The inputs to the jet algorithm were the four-momentum vectors of each calorimeter cell. The invariant mass of a jet, M_{jet}, was calculated from the sum of all four-momentum vectors assigned to the jet. The transverse energy of a jet was denoted by E_t^{jet}.

The $E-P_Z$ of the initial state is twice the positron beam energy, $2E_e=55$ GeV. For events that are fully contained in the calorimeter (ignoring particles escaping through the forward beam hole, which carry negligible $E-P_Z$), the measured $E-P_Z$ should be near $2E_e$. In photoproduction processes, where the final-state positron escapes through the rear beam hole, the $E-P_Z$ spectrum falls steeply, so that a cut on $E-P_Z$ is useful in reducing such backgrounds. Events with high-energy muons, which deposit only a small fraction of their energy in the calorimeter, will also have $E-P_Z$ substantially below $2E_e$. In the search for the $e\to\mu$ transition (see Secs. VI B and VI C), a cut was made on the quantity $E-P_Z+\Delta_\mu$, where $\Delta_\mu=\not{P}_t(1-\cos\theta_\mu)/\sin\theta_\mu$ is an estimate of the $E-P_Z$ carried by the muon, assuming that the transverse momentum of the muon is equal to $\not{P}_t$; θ_μ is the polar angle of the muon track.

VI. EVENT SELECTION FOR THE $e\to\mu$ TRANSITION

Events from the reaction $ep\to\mu X$, mediated by a heavy LQ, would be characterized by a high-transverse-momentum (P_t) muon balanced by a *jet*. Since only a small fraction of the muon energy is deposited in the calorimeter, these events would have a large $\not{P}_t$. The trigger selection, based on a $\not{P}_t$ request, was the same used in the CC DIS measurement [33]. The offline event selection consisted of two steps: a preselection of events with $\not{P}_t$ and a final selection requiring an identified muon.

A. Trigger selection

ZEUS has a three-level trigger system [19]. At the first trigger level, events were selected using criteria based on E_t and $\not{P}_t$. Typical threshold values were 5 GeV in $\not{P}_t$ or 11.5 GeV in E_t. At the second level, timing information from the calorimeter was used to reject events inconsistent with the bunch-crossing time. The $\not{P}_t$ was measured with a better resolution and a tighter cut of 6 GeV was applied. At the third level, track reconstruction and vertex finding are performed, allowing the rejection of candidate events with a vertex inconsistent with an *ep* interaction. The thresholds on the trigger quantities are considerably lower than the selection cuts applied in the off-line analysis.

B. Preselection

After applying cuts to further reject non-*ep* backgrounds (mainly cosmic rays and beam-gas interactions), the following preselection requirements were imposed:

a reconstructed vertex with Z coordinate $|Z_{\mathrm{VTX}}|<50$ cm;
$\not{P}_t>15$ GeV and $\not{P}_t/\sqrt{E_t}>2.5\sqrt{\mathrm{GeV}}$;
25 GeV $E-P_Z+\Delta_\mu<100$ GeV;
no electron with energy larger than 10 GeV.

The $\not{P}_t/\sqrt{E_t}$ cut mainly rejects photoproduction events with very high E_t. These events, due to the energy resolution of the calorimeter, could yield $\not{P}_t$ larger than the threshold but still have a low $\not{P}_t/\sqrt{E_t}$ value. The third cut further discriminates against photoproduction events, while the fourth cut suppresses NC DIS. The electron finder [34] is based on a neural-network algorithm. After the preselection, 164 events remained, compared with 177.3 ± 3.8 events predicted by the SM simulation normalized to the integrated luminosity of the data. The error associated with the prediction arises from the generated Monte Carlo (MC) statistics. The SM expectation is dominated by CC DIS, with small contributions from $ep\to e\mu^+\mu^-X$ and from W production. Simulated distributions of $E-P_Z+\Delta_\mu$, $\not{P}_t$, and $\not{P}_t/\sqrt{E_t}$ are compared with the data in Fig. 2. Good agreement is seen.

C. Muon identification

Two methods of muon identification were employed. The first, for very forward muons ($8°<\theta_\mu<20°$), required a reconstructed track in the FMUON detector with azimuth within 20° of ϕ_{miss}. In the second selection, for central muons ($15°<\theta_\mu<164°$), the following CAL- and CTD-based requirements were imposed:

a track that points to the vertex with transverse momentum (P_t^{trk}) above 5 GeV and an azimuth that differs from ϕ_{miss} by less than 20°;
no additional tracks with azimuth within 50° of ϕ_{miss} and $P_t^{trk}>1$ GeV;
the calorimeter energy deposits are consistent with those expected from a minimum ionizing particle in an (η,ϕ) cone of radius $R=0.3$, centered on the track;
muons with $115°<\theta_\mu<130°$ were excluded to eliminate the background from a very small fraction of electrons for which a large fraction of the energy was absorbed in the dead material between the BCAL and the RCAL.

After the muon identification, two events are left in the data, while the SM expectation is 1.43 ± 0.38, mainly from $ep\to e\mu^+\mu^-X$.

TABLE VI. The 95% C.L. upper limits on $\lambda_{eq_1}\sqrt{\beta_{lq}}$ for a leptoquark with mass $M_{\mathrm{LQ}}=250$ GeV.

LQ type	$\tilde{S}^L_{1/2}$	$S^L_{1/2}$	$S^R_{1/2}$	V^L_0/V^R_0	$\tilde{V}^R_0$	V^L_1
μ-channel limit on $\lambda_{eq_1\sqrt{\beta_{\mu q}}}$	0.10	0.038	0.036	0.081	0.029	0.020
τ-channel limit on $\lambda_{eq_1\sqrt{\beta_{\tau q}}}$	0.15	0.054	0.051	0.10	0.038	0.027

D. Final selection

The final selection was designed to reduce the SM background to a very low level. The following cuts were applied:

$\not{P}_t > 20$ GeV;

$\not{P}_t/\sqrt{E_t} > 4\sqrt{\mathrm{GeV}}$;

$E-P_Z+\Delta_\mu > 30$ GeV.

No event survived these cuts, while 0.40 ± 0.18 events are predicted by SM processes, mostly from $ep\to e\mu^+\mu^- X$.

VII. EVENT SELECTION FOR THE $e\to\tau$ TRANSITION

This channel is characterized by an isolated τ with high P_t balanced by a jet. Separate selections were made for hadronic τ decays (65%) and for the leptonic decays $\tau\to l\bar{\nu}_l\nu_\tau$ (35%). The same trigger as described in Sec. VI A was used. The offline event selection consisted of a pre-selection common to hadronic and leptonic τ decays and final selections specific to each decay mode of the τ. These mode-specific selections make use of the fact that one or more neutrinos are emitted in τ decay, producing $\not{P}_t$ approximately aligned with the τ. To produce a reasonably large event sample to compare with SM predictions, the selections for each τ decay mode were done in two steps.

A. Preselection

In addition to cuts to reject non-ep background, the preselection requirements were as follows:

a reconstructed vertex with Z coordinate $|Z_{\mathrm{VTX}}|<50$ cm;

$20\ \mathrm{GeV} < E-P_Z < 52$ GeV;

energy in RCAL <7 GeV.

The second cut reduces the photoproduction background. The third cut rejects NC DIS events where the positron was scattered into the RCAL.

B. Selection of hadronic τ decays

Events with a narrow ''pencil-like'' jet consistent with hadronic τ decay were selected with the following requirements:

the transverse energy of the jet associated with the τ should satisfy $E_t^{\tau-\mathrm{jet}} \gg 10$ GeV;

$M_{\mathrm{jet}} \ll 7$ GeV;

1, 2, or 3 tracks associated with the jet;

the number of calorimeter cells associated with the jet, N_{cells}, is at least 10 (to suppress electrons) and at most 50 (to ensure that the jet is narrow);

$R_{90\%} \leqslant 0.3$, where $R_{90\%}$ is the radius of the (η, ϕ) cone centered on the jet axis that contains 90% of the jet energy;

$f_{\mathrm{EMC}} \ll 0.95$, where f_{EMC} is the fraction of the jet energy deposited in the electromagnetic section of the calorimeter;

$f_{\mathrm{EMC}}+f_{\mathrm{LT}}<1.6$, where f_{LT} is the momentum of the most-energetic track in the jet divided by the jet energy (leading-track fraction).

The last two cuts reject electrons, for which $f_{\mathrm{EMC}}\sim 1$ and $f_{\mathrm{LT}}\sim 1$. After these cuts, 367 data events were selected in comparison to 377.7 ± 12.5 from the SM expectation (mainly from NC DIS, CC DIS, and photoproduction). Figure 3 shows several distributions of characteristic variables of the τ candidates at this stage of the analysis. The SM simulation provides a reasonable description of the data.

The final stage of the hadronic τ-decay selection requires events consistent with a two-body τ+jet final state:

$E_t^{\tau-\mathrm{jet}} \gg 20$ GeV;

the azimuthal angle of the τ candidate is within 20° of ϕ_{miss};

$\not{P}_t \gg 12$ GeV;

at least one additional jet with $E_t^{\mathrm{jet}} \gg 25$ GeV.

No candidate satisfying these requirements was found, while 0.62 ± 0.18 events are expected from SM processes.

C. Selection of $\tau\to\mu\bar{\nu}_\mu\nu_\tau$ decays

After the preselection described in Sec. VII A, events with an isolated high-P_t muon balanced by a jet were selected. Isolated muon candidates were identified using a neural-network algorithm that analyzed the pattern of longitudinal and transverse energy deposition in the calorimeter and matching track(s) in the CTD and/or the muon chambers. Since the energy deposited in the CAL by the muon is typically a small fraction of the energy of the τ, cuts on $\not{P}_t$ were applied. The initial requirements were as follows:

a muon with $P_t > 10$ GeV and $8° < \theta_\mu < 125°$;

$\not{P}_t > 15$ GeV;

$\not{P}_t/\sqrt{E_t} > 4\sqrt{\mathrm{GeV}}$;

a jet with $E_t^{\mathrm{jet}} > 25$ GeV;

events with an identified electron [35] with energy greater than 10 GeV were vetoed.

The last cut reduces the NC DIS background. Figures 4(a) and 4(b) show the distributions of $E-P_Z$ and $\not{P}_t$ for the $\tau\to\mu\bar{\nu}\nu$ candidates after these cuts, compared to the SM background. Good agreement is observed. After these cuts, 119 data events remained, compared to 107.2 ± 7.4 events from the SM expectation (mainly CC DIS and photoproduction).

The final selection consisted of two cuts:

$\not{P}_t > 20$ GeV;
the muon azimuth differs from $\phi_{\rm miss}$ by less than 20°.

No event passed the final selection, while 0.23 ± 0.07 events were expected from SM processes.

D. Selection of $\tau \to e \bar{\nu}_e \nu_\tau$ decays

After the preselection described in Sec. VII A, events with an isolated electron and a jet were selected by imposing the following requirements:

an identified electron [35] with energy greater than 20 GeV and the polar angle θ_e satisfying $8° < \theta_e < 125°$;
$\not{P}_t \gg 10$ GeV;
$\not{P}_t / \sqrt{E_t} > 2\sqrt{\rm GeV}$;
a jet with $E_t^{\rm jet} > 25$ GeV.

Figures 4(c) and 4(d) show the distributions of $E - P_Z$ and $\not{P}_t$ for the $\tau \to e \bar{\nu} \nu$ candidates that satisfied these requirements, where 116 data events were selected and 109.1 ± 5.4 events from SM backgrounds were expected (mainly NC DIS and photoproduction).

The final selection consisted of a higher $\not{P}_t$ cut and a requirement that the lepton and the jet be back-to-back:

$\not{P}_t > 15$ GeV;
the azimuth of the electron differs from $\phi_{\rm miss}$ by less than 20°.

No event passed the final selection, while 0.32 ± 0.10 events were expected from SM processes.

VIII. EFFICIENCIES

The selection efficiencies were evaluated using signal MC events (see Sec. IV). For resonant production of lepton-flavor-violating scalar LQs, the μ-channel selection efficiency falls from 60% to 52% as $M_{\rm LQ}$ increases from 140 GeV to 280 GeV, while the efficiency for vector LQs drops from 64% to 56%. For $M_{\rm LQ} \gg 240$ GeV, the FMUON-based muon selection increases the selection efficiency by about 20% compared to the CAL-CTD-based selection alone. Over the $M_{\rm LQ}$ interval from 140 GeV to 280 GeV, the selection efficiency for LQs that couple to τ increases from 24% to 31% for scalar LQs and from 21% to 33% for vector LQs.

For LQs with $M_{\rm LQ} \gg \sqrt{s}$, the efficiencies are almost independent of $M_{\rm LQ}$, but depend strongly on the generation of the initial-state quark. For $e \to \mu$ transitions, the selection efficiency ranges from 15% to 45% for $F = 0$ LQs and from 15% to 35% for $|F| = 2$ LQs. For $e \to \tau$ transitions, the efficiencies are lower and range from 5% to 19% for $F = 0$ LQs and from 4% to 16% for $|F| = 2$ LQs. When the initial-state quark is a sea quark and especially for *s*, *c*, or *b* quarks, the efficiency is considerably lower than for valence quarks due to the softer *x* spectrum, which results in a lower transverse momentum for the final-state lepton.

IX. RESULTS

Since no candidate for LFV processes was found, limits were set on these processes. All limits were evaluated at 95% confidence level (C.L.) using a Bayesian approach, assuming a flat prior for the signal cross section. Systematic uncertainties in the detector simulation and in the integrated luminosity (see Sec. IX A) were taken into account using a method described elsewhere [36]. For low-mass LQs with narrow width, the branching ratio β was regarded as a free parameter and limits were set on $\sigma \beta_{lq}$. These limits were converted to limits on $\lambda_{eq_1} \sqrt{\beta_{lq}}$ using Eq. (1) corrected for QED-ISR and NLO QCD (only for scalar LQs). For high-mass leptoquarks, the cross-section limit was converted to a limit on $\lambda_{eq_\alpha} \lambda_{lq_\beta} / M_{\rm LQ}^2$ using Eq. (2) with QED-ISR corrections. The CTEQ4 [37] parametrizations of parton densities were used to evaluate cross sections.

A. Systematic uncertainties

The uncertainty on the integrated luminosity is 1.6%. Systematic uncertainties of 3% on the CAL energy scale and 10% on the CAL response to muons were taken into account. The resulting variations on the efficiency for the muon (tau) channel were 3% (4%) for low-mass LQs and up to 15% (17%) for high-mass LQs that couple to *b* quarks in the initial state.

Systematic uncertainties in the cross-section evaluation related to the choice of parton density function (PDF) were investigated using Martin-Roberts-Sterling-Thorne (MRST) sets [38] as an alternative choice to CTEQ4. The main differences were found for low-mass LQs with masses close to $\sqrt{s}$ when very high-*x* quarks are involved. In these cases, limits calculated using MRST were stricter than the CTEQ4-based limits presented here. Another possible source of uncertainties for vector and high-mass scalar LQs are the unknown NLO-QCD cross-section corrections (see Sec. II A).

B. Low-mass LQ and squark limits

Figure 5 shows upper limits on $\sigma \beta_{\mu q}$ and $\sigma \beta_{\tau q}$. For $e \to \mu$, the search is sensitive to processes with cross sections as low as 0.1 pb, while for $e \to \tau$, the sensitivity is 0.2–0.3 pb. These limits apply generally to narrow resonances with LFV decay modes, for example, to the $\not{R}_p$ squarks described in Sec. II B.

Upper limits on $\lambda_{eq_1} \sqrt{\beta_{lq}}$ have been derived for $F = 0$ LQs by assuming resonantly produced LQs described by the BRW model. These limits can be applied to processes involving any quark generations in the final state (excluding the *t* quark). Figures 6(a) and 6(b) show the upper limits on $\lambda_{eq_1} \sqrt{\beta_{\mu q}}$ for scalar and vector LQs, respectively. Under the assumption that $\lambda_{eq_1} = \lambda_{\mu q_\beta}$, limits on λ_{eq_1} can be derived. These are compared to limits from low-energy experiments in Figs. 6(c) and 6(d) for $S_{1/2}^L$ and V_0^R LQs. These states do not couple to neutrinos and therefore $\beta_{\mu q} = 0.5$. For $M_{\rm LQ} < 250$ GeV, the ZEUS limits are stronger than the low-energy limits for LQs that couple to μ and *b*. Limits on $\lambda_{eq_1} \sqrt{\beta_{\tau q}}$ are shown in Figs. 7(a) and 7(b). Figures 7(c) and

7(d) show the corresponding limits on λ_{eq_1}, assuming $\lambda_{eq_1}=\lambda_{\tau q_\beta}$ (and therefore $\beta_{\tau q}=0.5$). The ZEUS limits are more stringent than the limits from low-energy experiments over a wide mass range, with the exception of limits from $K^+\to\pi^+\nu\overline{\nu}$ [39]. As described in Sec. II B, the limits on $\lambda_{eq_1}\sqrt{\beta_{lq}}$ for $\tilde{S}^L_{1/2}$ can be interpreted as limits on $\lambda'_{1j1}\sqrt{\beta_{\tilde{u}^j\to lq}}$ for $\tilde{u}^j$ squarks.

Another way to illustrate the sensitivity is to assume that the couplings have electromagnetic strength ($\lambda_{eq_1}=\lambda_{lq_\beta}=0.3\approx\sqrt{4\pi\alpha}$). In this case, LQs with masses up to 283 GeV are excluded, as shown in Table V. Alternatively, as shown in Table VI, for a fixed $M_{\rm LQ}$ of 250 GeV, values of $\lambda_{eq_1}\sqrt{\beta_{lq}}$ down to 0.020 (0.027) for $LQ\to\mu q$ ($LQ\to\tau q$) are excluded. The CDF [40] and Dø [41] collaborations exclude scalar LQs with $M_{\rm LQ}<202$ GeV and $M_{\rm LQ}<200$ GeV, respectively, at 95% C.L. with $\beta_{\mu q}=100\%$. CDF [42] excludes $M_{\rm LQ}<99$ GeV with $\beta_{\tau b}=100\%$. The ZEUS limits are complementary to those of the Tevatron in the sense that the latter are independent of the Yukawa couplings and assume that LQs couple to a single lepton generation.

C. High-mass LQ and squark limits

For $M_{\rm LQ}\gg\sqrt{s}$, limits on $\lambda_{eq_\alpha}\lambda_{lq_\beta}/M^2_{\rm LQ}$ were evaluated for all combinations of quark generations (α, β). Tables I and II show these limits for $F=0$ and $|F|=2$ LQs, respectively, that couple to μq_β. Tables III and IV show the corresponding limits for the LQs coupling to τq_β. In many cases involving c and b quarks, the ZEUS limits improve on the low-energy limits [8,43,44]. Limits obtained by H1 [10] are comparable to the ZEUS limits.

The limits on $\lambda_{eq_\alpha}\lambda_{lq_\beta}/M^2_{\rm LQ}$ for $\tilde{S}^L_{1/2}$ can be interpreted as limits on $\lambda'_{1j\alpha}\lambda'_{ij\beta}/M^2_{\tilde{u}}$ for a u-type squark of generation j, where $l=\mu$ or τ for $i=2$ or 3, respectively. Similarly, the limits on S^L_0 LQs can be interpreted as limits on $\lambda'_{1\alpha k}\lambda'_{i\beta k}/M^2_{\tilde{d}}$ for a d-type squark of generation k.

X. CONCLUSIONS

A search for lepton-flavor violation has been performed with 47.7 pb^{-1} of e^+p data at $\sqrt{s}=300$ GeV collected with the ZEUS detector at HERA in 1994–1997. Both the μ and τ channels have been analyzed. No evidence for LFV processes has been found.

Limits at 95% C.L. on cross sections, couplings, and masses for $F=0$ LQs that mediate LFV processes have been set. Assuming the couplings $\lambda_{eq_1}=\lambda_{lq_\beta}=0.3$, lower mass limits between 258 and 283 GeV have been derived for various LQs decaying to μq or τq. For $M_{\rm LQ}=250$ GeV, upper limits for $\lambda_{eq_1}\sqrt{\beta_{\mu q}}$ in the range $(2.0-10)\times10^{-2}$ and for $\lambda_{eq_1}\sqrt{\beta_{\tau q}}$ in the range $(2.7-15)\times10^{-2}$ were obtained. Limits on $\tilde{S}^L_{1/2}$ also apply to up-type squarks that have R-parity-violating couplings to both a positron and either a μ or a τ.

For LQs with $M_{\rm LQ}\gg\sqrt{s}$, upper limits on $\lambda_{eq_\alpha}\lambda_{lq_\beta}/M^2_{\rm LQ}$ have been obtained and compared with bounds from low-energy experiments. Some of these limits also apply to high-mass R_p-violating squarks. A number of ZEUS limits are the most stringent published to date, especially for $e\to\tau$ transitions.

ACKNOWLEDGMENTS

The strong support and encouragement of the DESY directorate have been invaluable. The experiment was made possible by the inventiveness and the diligent efforts of the HERA machine group. The design, construction, and installation of the ZEUS detector have been made possible by the ingenuity and dedicated efforts of many people from inside DESY and from the home institutes who are not listed as authors. Their contributions are acknowledged with great appreciation. We acknowledge support by the following: the Natural Sciences and Engineering Research Council of Canada (NSERC); the German Federal Ministry for Education and Science, Research and Technology (BMBF), under contract numbers HZ1GUA 2, HZ1GUB 0, HZ1PDA 5, HZ1VFA 5; the MINERVA Gesellschaft für Forschung GmbH, the Israel Science Foundation, the U.S.–Israel Binational Science Foundation, the Israel Ministry of Science and the Benozyio Center for High Energy Physics; the German-Israeli Foundation, the Israel Science Foundation, and the Israel Ministry of Science; the Italian National Institute for Nuclear Physics (INFN); the Japanese Ministry of Education, Science and Culture (the Monbusho) and its grants for Scientific Research; the Korean Ministry of Education and Korea Science and Engineering Foundation; the Netherlands Foundation for Research on Matter (FOM); the Polish State Committee for Scientific Research, grant no. 115/E-343/SPUB-M/DESY/P-03/DZ 121/2001-2002 and by the German Federal Ministry for Education and Science, Research and Technology (BMBF); the Fund for Fundamental Research of Russian Ministry for Science and Education and by the German Federal Ministry for Education and Science, Research and Technology (BMBF); the Spanish Ministry of Education and Science through funds provided by (CICYT); the Particle Physics and Astronomy Research Council, UK; the U.S. Department of Energy; the U.S. National Science Foundation. J. Rautenberg was supported by the GIF, contract I-523-13.7/97. D.S. Bailey and N. H. Brook acknowledge financial support from the PPARC. E. Rodriguez and R. Gonçalo were supported by the Portuguese Foundation for Science and Technology (FCT). A. M. Kowal was supported by the Polish State Committee for Scientific Research, grant no. 5 P-03B 13720. J. Szuba was partly supported by the Israel Science Foundation and the Israel Ministry of Science. I. Redondo was supported by the Comunidad Autonoma de Madrid. L. Adam'czyk and P. R. B. Saull were partly supported by Tel Aviv University. B. Smalska was supported by the Polish State Committee for Scientific Research, grant no. 2 P-03B 00219. T. Tymieniecka and A. Ukleja were supported by the Polish State Committee for Scientific Research, grant no. 5 P-03B 09820, and by the German Federal Ministry for Education and Research (BMBF), grant no. POL 01/043. L. K. Gladilin was partly supported by University of Wisconsin via the U.S.–Israel BSF.

[1] Super-Kamiokande Collaboration, Y. Fukuda *et al.*, Phys. Rev. Lett. **81**, 1562 (1998).
[2] SNO Collaboration, Q. R. Ahmad *et al.*, Phys. Rev. Lett. **87**, 071301 (2001).
[3] Z. Maki, M. Nakagawa, and S. Sakata, Prog. Theor. Phys. **28**, 870 (1962); P. Fisher, B. Kayser, and K. S. McFarland, Annu. Rev. Nucl. Part. Sci. **49**, 481 (1999).
[4] J. C. Pati and A. Salam, Phys. Rev. D **10**, 275 (1974); H. Georgi and S. L. Glashow, Phys. Rev. Lett. **32**, 438 (1974); P. Langacker, Phys. Rep. **72**, 185 (1981).
[5] H. P. Nilles, Phys. Rep. **110**, 1 (1984); H. E. Haber and G. L. Kane, *ibid.* **117**, 75 (1985).
[6] B. Schrempp and F. Schrempp, Phys. Lett. **153B**, 101 (1985); J. Wudka, Phys. Lett. **167B**, 337 (1986).
[7] S. Dimopoulos and L. Susskind, Nucl. Phys. **B155**, 237 (1979); S. Dimopoulos, *ibid.* **B168**, 69 (1980); E. Farhi and L. Susskind, Phys. Rev. D **20**, 3404 (1979); Phys. Rep. **74**, 277 (1981).
[8] S. Davidson, D. Bailey, and B. A. Campbell, Z. Phys. C **61**, 613 (1994).
[9] ZEUS Collaboration, M. Derrick *et al.*, Z. Phys. C **73**, 613 (1997).
[10] H1 Collaboration, C. Adloff *et al.*, Eur. Phys. J. C **11**, 447 (1999); **14**, 553 (2000).
[11] W. Buchmüller, R. Rückl, and D. Wyler, Phys. Lett. B **191**, 442 (1987); **448**, 320E (1999).
[12] A. Djouadi *et al.*, Z. Phys. C **46**, 679 (1990).
[13] T. Plehn *et al.*, Z. Phys. C **74**, 611 (1997).
[14] Z. Kunszt and W. J. Stirling, Z. Phys. C **75**, 453 (1997).
[15] C. F. von Weizsäcker, Z. Phys. **88**, 612 (1934).
[16] E. J. Williams, Phys. Rev. **45**, 729 (1934).
[17] V. Barger, G. F. Giudice, and T. Han, Phys. Rev. D **40**, 2987 (1989).
[18] J. Butterworth and H. Dreiner, Nucl. Phys. **B397**, 3 (1993).
[19] ZEUS Collaboration, *The ZEUS Detector*, DESY Status Report, 1993 edited by U. Holm, available on http://www-zeus.desy.de/bluebook/bluebook.html
[20] N. Harnew *et al.*, Nucl. Instrum. Methods Phys. Res. A **279**, 290 (1989); B. Foster *et al.*, Nucl. Phys. B (Proc. Suppl.) **32**, 181 (1993); Nucl. Instrum. Methods Phys. Res. A **338**, 254 (1994).
[21] M. Derrick *et al.*, Nucl. Instrum. Methods Phys. Res. A **309**, 77 (1991); A. Andresen *et al.*, *ibid.* **309**, 101 (1991); A. Caldwell *et al.*, *ibid.* **321**, 356 (1992); A. Bernstein *et al.*, *ibid.* **336**, 23 (1993).
[22] J. Andruszków *et al.*, Report DESY-92-066, DESY, 1992; ZEUS Collaboration, M. Derrick *et al.*, Z. Phys. C **63**, 391 (1994); J. Andruszków *et al.*, Preprint DESY-01-041, 2001.
[23] S. B. Silverstein, Ph.D. thesis, Wisconsin University, Madison, 1996.
[24] L. Bellagamba, Comput. Phys. Commun. **141**, 83 (2001).
[25] T. Sjöstrand, Comput. Phys. Commun. **82**, 74 (1994).
[26] K. Charchula, G. A. Schuler, and H. Spiesberger, Comput. Phys. Commun. **81**, 381 (1994).
[27] L. Lönnblad, Comput. Phys. Commun. **71**, 15 (1992).
[28] J. A. M. Vermaseren, Nucl. Phys. **B229**, 347 (1983).
[29] U. Baur, J. A. M. Vermaseren, and D. Zeppenfeld, Nucl. Phys. **B375**, 3 (1992).
[30] G. Marchesini *et al.*, Comput. Phys. Commun. **67**, 465 (1992).
[31] R. Brun *et al.*, GEANT3, Technical Report CERN-DD/EE/84-1, CERN, 1987.
[32] ZEUS Collaboration, J. Breitweg *et al.*, Eur. Phys. J. C **2**, 61 (1998).
[33] ZEUS Collaboration, J. Breitweg *et al.*, Eur. Phys. J. C **12**, 411 (2000).
[34] H. Abramowicz, A. Caldwell, and R. Sinkus, Nucl. Instrum. Methods Phys. Res. A **365**, 508 (1995).
[35] ZEUS Collaboration, J. Breitweg *et al.*, Eur. Phys. J. C **11**, 427 (1999).
[36] M. Corradi, *Proceedings of the Workshop on Confidence Limits* (CERN, Geneva, Switzerland, 2000), p. 237. Also in preprint CERN 2000-005, available on http://cern.web.cern.ch/CERN/Divisions/EP/Events/CLW/PAPERS/PS/corradi.ps
[37] H. L. Lai *et al.*, Phys. Rev. D **55**, 1280 (1997).
[38] A. D. Martin *et al.*, Eur. Phys. J. C **4**, 463 (1998).
[39] E787 Collaboration, S. Adler *et al.*, Phys. Rev. Lett. **84**, 3768 (2000).
[40] CDF Collaboration, F. Abe *et al.*, Phys. Rev. Lett. **81**, 4806 (1998).
[41] DØ Collaboration, B. Abbott *et al.*, Phys. Rev. Lett. **84**, 2088 (2000).
[42] CDF Collaboration, F. Abe *et al.*, Phys. Rev. Lett. **78**, 2906 (1997).
[43] E. Gabrielli, Phys. Rev. D **62**, 055009 (2000).
[44] Particle Data Group, D. E. Groom *et al.*, Eur. Phys. J. C **15**, 1 (2000).